Comparison of the characteristic of heat transport between non-shear and shear systems at solid-liquid (S-L) interfaces

Abdul Rafeq Bin Saleman[1,2,*], Fudhail Abdul Munir[1,2], Mohd Fadzli Bin Abdollah[1,2], Gota Kikugawa[3], Taku Ohara[3]

[1)] Faculty of Mechanical Engineering, Universiti Teknikal Malaysia Melaka, Hang Tuah Jaya, 76100 Durian Tunggal, Melaka, Malaysia.
[2)] Centre for Advanced Research on Energy, Universiti Teknikal Malaysia Melaka, Hang Tuah Jaya, 76100 Durian Tunggal, Melaka, Malaysia.
[3)] Institute of Fluid Science, Tohoku University, 2-1-1 Katahira Aoba-ku, Sendai 980-8577, Japan.

[*]Corresponding e-mail: rafeq@utem.edu.my

Keywords: Solid-liquid interfaces; molecular heat transfer; simple liquid

ABSTRACT – Heat transport at solid-liquid (S-L) interfaces play an important role in determining the performance of a system. Although there are several studies conducted related to the characteristics of heat transport at S-L interface, the comparison between non-shear and shear heat transport have yet to be explored thoroughly. This study will look into the heat transport characteristics between non-shear system and shear system based on the thermal boundary resistance. It is found that, surface structure of solid walls and shear system have influences on the characteristics of heat transport at S-L interfaces.

1. INTRODUCTION

Solid-liquid (S-L) interfaces was utilized in various engineering applications such a lubrication and coatings systems [1]. In the lubrication and coating systems, heat transport play a significant role in the performance of the system [2-3]. A system generally will fail without adequate thermal management. As such, the knowledge of the heat transport is crucial in a system. Although there are a number of investigation done related to heat transport [4–6] at S-L interfaces, the clear view of heat transport between shear system and non-shear system have yet to be clarify thoroughly. Therefore, this study investigated the comparison of the heat transport at S-L interfaces between non-shear and shear systems using molecular dynamics simulation.

2. SIMULATION SYSTEM

The simulation system consists of liquid confined between two parallel solid walls as shown in Figure 1. The liquid is a simple liquid. The solid walls consisted of face-centred cubic (FCC) lattice with three types of surfaces which is (100), (110) and (111) facing the liquid. The three types of surfaces for the FCC lattice is shown in Figure 2.

2.1 Potential functions

The simple liquid was modelled using Lennard Jones 12-6 (LJ) potentials which is given as follows [7]:

$$U^{LJ}(r_{ij}) = 4\varepsilon_{ij}\left[\left(\frac{\sigma_{ij}}{r_{ij}}\right)^{12} - \left(\frac{\sigma_{ij}}{r_{ij}}\right)^{6}\right] \quad (1)$$

The ε and σ is 2.0433 × 10 and 3.73A, respectively. The parameter for methane is utilized in this system. As for the solid wall, it is modelled by Morse potentials [8]:

$$\Phi(r_{ij}) = D[e^{-2\alpha(r_{ij}-r_o)} - 2e^{-\alpha(r_{ij}-r_o)}] \quad (2)$$

Where the parameters were D = 7.6148 × 10^{-20} J, r_0 = 3.0242 Å and α = 1.5830 $Å^{-1}$, which the parameter for gold. The interaction between solid and liquid molecules was modelled by LJ potential. The interaction parameters were calculated using Lorent-Bertholet combining rules which is given as follow [6]:

$$\varepsilon_{sl} = \sqrt{\varepsilon_{ss}\varepsilon_{ll}} \quad \text{and} \quad \sigma_{sl} = \frac{\sigma_{ss} + \sigma_{ll}}{2} \quad (3)$$

The interaction sites *s* and *l* belong to solid and liquid respectively. The interactions were cut-off beyond the radius of 12.0 Å for the Morse and LJ potentials. The size of the simulation system was approximately 40 × 40 × 120 Å and a periodic boundary condition was applied in the *x*- and *y*-directions of the simulation systems

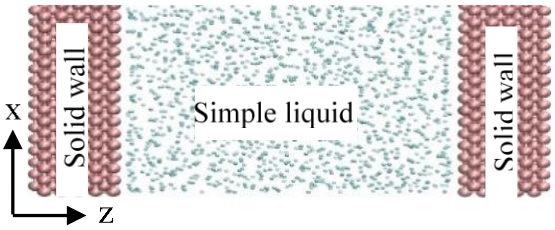

Figure 1 The system of liquid confined between two solid walls.

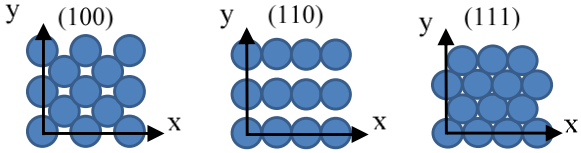

Figure 2 FCC lattices of (100), (110) and (111).

2.2 Simulation details

The reversible references propagator algorithm (r-RESPA) was applied for the time integration [9]. Initially the temperature of the system was raised to the targeted temperature of 0.7 T_c (critical temperature) of the liquid and the system is equilibrated until a uniform temperature is acquired. Then the non-shear and shear was setup and

run until equilibrium. In the non-shear setup, the solid walls were set at low temperature and at the center of the liquid, high temperature was set. As for the shear system, a constant speed of 100 m/s was applied to the two solid walls in the opposite directions generating sheared liquid. Finally, the heat flux (HF) across the simulation system is measured. The value of HF is tabulated in Table 1 and Table 2 for non-shear and shear system respectively.

Table 1 Non-shear system.

Crystal Plane	TJ (K)	HF (MW/m2)	TBR x 10^{-6} (m^2K/W)
100	22.9	188.9	0.1215
110	17.2	190.0	0.0907
111	19.5	188.8	0.1031

Table 2 Shear system.

Crystal Plane	TJ (K)	HF (MW/m2)	TBR x 10^{-6} (m^2K/W)
100	13.0	86.3	0.1503
110	17.5	181.6	0.0963
111	9.0	58.3	0.1551

3. RESULTS AND DISCUSSION

3.1 Temperature distributions

In order to calculate the temperature distributions of the system, the simulation system was divided into several slabs as mentioned in ref [9]. The temperature of each slab was calculated from the kinetic energy of the random velocity of molecules. Figure 3 shows the temperature distribution of the simulation system.

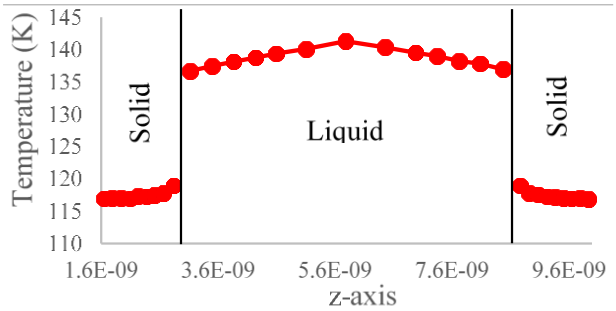

Figure 3 Temperature distributions for (110) crystal plane of non-shear system.

Based on Figure 3, temperature jump (TJ) is observed on the left and right sides of the S-L interfaces. TJ is defined as the temperature discontinuity at the S-L interfaces. Similar tendency is observed for all types of crystal planes for both shear and non-shear system, where there exist TJ at the S-L interfaces. The value of TJ at S-L interfaces for all types of FCC for the cases of non-shear and shear systems is tabulated in Table 1 and Table 2 for the non-shear and shear systems, respectively. Based on the value of TJ for the non-shear system, the TJ is in the order of (110), (111) and (100) crystal planes starting from the smallest to the largest. As for shear system the order is (111), (100) and (110). Based on this finding it is understood that different surface structure generates different TJ which will leads to different characteristics of heat transport.

3.2 Thermal boundary resistance (TBR)

In order to understand the characteristics of heat transport at S-L interfaces the TBR is determined, which is defined as follow [6]:

$$\mathrm{TBR} = \frac{TJ}{HF} \tag{4}$$

Where *HF* and *TJ* are the heat flux and temperature jump at the S-L interface, respectively. The calculated value of TBR is tabulated in Table 1 and Table 2. Based on Table 1 and Table 2, The TBR is in the order of (110), (111) and (100) for the non-shear system start from the lowest to the highest. As for shear system, it is in the order of (110), (100) and (111). From this observation it is understood that sheared liquid influences the characteristics of heat transport at S-L interfaces.

4. CONCLUSION

Shear system and surface structure of solid wall influences significantly the heat transport characteristics at S-L interfaces.

ACKNOWLEDGEMENT

The author, Abdul Rafeq Bin Saleman gratefully acknowledge Universiti Teknikal Malaysia Melaka and Ministry of Higher Education Malaysia for the scholarship during his PhD study at Tohoku Univerity, Japan.

REFERENCES

[1] Abdullah, M. I. H. C., Abdollah, M. F. B., Amiruddin, H., Nuri, N. R. M., Tamaldin, N., Hassan, M., & Rafeq, S. A. (2014). Effect of hBN/Al_2O_3 nanoparticles on engine oil properties. *Energy Education Science and Technology Part A: Energy Science and Research*, *32*(5), 3261-3268.

[2] Voevodin, A. A., Muratore, C., & Aouadi, S. M. (2014). Hard coatings with high temperature adaptive lubrication and contact thermal management. *Surface and Coatings Technology*, *257*, 247-265.

[3] Chung, P. S., Jhon, M. S., & Choi, H. J. (2016). Molecularly thin fluoro-polymeric nanolubricant films: tribology, rheology, morphology, and applications. *Soft matter*, *12*(11), 2816-2825.

[4] Amani, A., Karimian, S. M. H., & Seyednia, M. (2017). A molecular dynamics simulation on the effect of different parameters on thermal resistance of graphene-argon interface. *Molecular Simulation*, *43*(4), 276-283.

[5] Kim, B. H., Beskok, A., & Cagin, T. (2008). Molecular dynamics simulations of thermal resistance at the liquid-solid interface. *The Journal of Chemical Physics*, *129*(17), 174701.

[6] Bin Saleman, A. R., Chilukoti, H. K., Kikugawa, G., Shibahara, M., & Ohara, T. (2017). A molecular dynamics study on the thermal transport properties and the structure of the solid–liquid interfaces between face centered cubic (FCC) crystal planes of gold in contact with linear alkane liquids. *International Journal of Heat and Mass Transfer*, *105*, 168-179.

[7] Eggimann, B. L., Siepmann, J. I., & Fried, L. E. (2007). Application of the TraPPE force field to predicting isothermal pressure–volume curves at high pressures and high temperatures. *International Journal of Thermophysics*, *28*(3), 796-804.

[8] Boccara, N. (2007). The Morse Potential. *Essentials of Mathematica: With Applications to Mathematics and Physics*, 445-448.

[9] Bin Saleman, A. R., Chilukoti, H. K., Kikugawa, G., Shibahara, M., & Ohara, T. (2017). A molecular dynamics study on the thermal energy transfer and momentum transfer at the solid-liquid interfaces between gold and sheared liquid alkanes. *International Journal of Thermal Sciences*, *120*, 273-288.